JOURNAL OF AIRCRAFT
Vol. 34, No. 1, January–February 1997

Design of Subscale Airfoils with Full-Scale Leading Edges for Ice Accretion Testing

Farooq Saeed,* Michael S. Selig,† and Michael B. Bragg‡
University of Illinois at Urbana–Champaign, Urbana, Illinois 61801

A design procedure for subscale airfoils with full-scale leading edges that exhibit full-scale water droplet impingement characteristics in an incompressible, inviscid flow is presented. The design procedure uses validated airfoil design, flow analysis, and water droplet impingement simulation codes to accomplish the task. To identify and isolate important design variables in the design, numerous trade studies were performed. This paper presents the results of the trade studies and briefly discusses the role of important design variables in the subscale airfoil design. The effect of these design variables on circulation, velocity distribution, and impingement characteristics is discussed along with the accompanying implications and compromises in the design. A strategy to incorporate viscous effects into the design is also presented. This article also presents the design of a half-scale airfoil model with a 5% upper and 20% lower full-scale surface of the Learjet 305 airfoil leading edge and compares its aerodynamic as well as the droplet impingement characteristics with that of the Learjet 305 airfoil.

Nomenclature

C_l = airfoil lift coefficient
c = airfoil chord length
c_{m0} = airfoil zero-lift pitching moment coefficient at $c/4$
F_r = Froude number, $V_\infty/\sqrt{cg}$
K = droplet inertia parameter, $\rho_w\delta^2 V_\infty/18c\mu$
K_S = trailing-edge thickness parameter
M = freestream Mach number
Re = freestream Reynolds number, $\rho V_\infty c/\mu$
R_U = droplet freestream Reynolds number, $\rho\delta V_\infty/\mu$
S = airfoil surface arc length measured from the leading edge where $S = 0$
T = freestream static temperature
V = surface velocity
V_∞ = freestream velocity
x, y = airfoil coordinates
$x_m, \bar{x}_m$ = upper and lower surface match locations
$x_r, \bar{x}_r$ = upper and lower surface pressure recovery locations
x_0, y_0 = initial horizontal and vertical displacement of the droplet
v_1 = design velocity level for segment 1
α = angle of attack relative to the chord line
α_e = effective angle of attack relative to the nose section chord line, $\alpha - \gamma$
$\alpha^*, \bar{\alpha}^*$ = upper and lower surface multipoint design angle-of-attack distribution
β = local impingement efficiency
Γ = circulation strength normalized by $V_\infty c_{fs}$
$\bar{\Gamma}$ = circulation strength, m^2/s
γ = nose droop angle
δ = droplet diameter
η = normalized subscale airfoil chord length, c_{ss}/c_{fs}
μ = air viscosity
ρ = air density
ρ_w = water density
τ = finite trailing-edge angle
ϕ_{le} = leading-edge arc limit

Subscripts
fs = full-scale airfoil
i = inviscid
l = lower surface
ss = subscale airfoil
u = upper surface
v = viscous

Presented as Paper 96-0635 at the AIAA 34th Aerospace Sciences Meeting, Reno, NV, Jan. 15–19, 1996; received March 31, 1996; revision received Sept. 14, 1996; accepted for publication Sept. 15, 1996.

*Graduate Research Assistant, Department of Aeronautical and Astronautical Engineering, 306 Talbot Laboratory, 104 South Wright Street. Student Member AIAA.

†Assistant Professor, Department of Aeronautical and Astronautical Engineering, 306 Talbot Laboratory, 104 South Wright Street. Member AIAA.

‡Professor, Department of Aeronautical and Astronautical Engineering, 306 Talbot Laboratory, 104 South Wright Street. Associate Fellow AIAA.

Introduction

RECENT aircraft accidents have raised important flight safety issues related to the effect of ice accretion on airfoil and wing performance. To improve flight safety, a better understanding of the effect of ice accretion on the aerodynamic performance of modern airfoils is required. One important step in this process is to evaluate the aerodynamic performance of the airfoil sections (or the wing as a whole) at the icing conditions within the certification icing envelop that result in the largest performance penalties.

Since ice accretion scaling is still not well understood, testing at full-scale or near full-scale conditions is highly desirable. The available ice accretion tunnels, however, are too small to test full-scale airfoils or wings of most aircraft of interest. Numerous investigators have performed experimental or analytical studies[1–5] in an effort to evaluate full-scale ice protection systems for wing sections using truncated airfoil models. These truncated airfoil models use a full-scale leading-edge section followed by a faired or flapped aft section that, in effect, reduces the overall length or chord of the model. To our knowledge, however, no systematic study has been performed to provide insight into the design of the aft section.

With these issues in mind, a subscale model design procedure was formulated with the objective of providing design guidance for subscale models that simulate full-scale water droplet impingement characteristics. The formulation was based on the fact that the leading-edge ice accretion will be

the same between the subscale and full-scale airfoils if cloud properties, droplet impingement, local leading-edge flowfield, model surface geometry, model surface quality, and model surface thermodynamic characteristics are the same. Using the fact that ice usually accretes only on the airfoil leading edge, where the supercooled water droplets impinge, the subscale airfoil model is designed with a leading-edge geometry (first 10–20% of chord) identical to that of the full-scale leading edge. The design of the aft section is such that it provides full-scale flowfield and droplet impingement on the leading edge. With this approach, the effect of various design variables on the inviscid flowfield and droplet impingement characteristics of the subscale airfoil was examined to obtain useful guidelines for the design. The final design is based on viscous considerations as well.

The model design procedure for full-scale flowfield and droplet impingement simulation uses validated computational airfoil aerodynamics and droplet impingement codes,[6–13] specifically, an inverse design method,[8] the Eppler code,[6,7] XFOIL,[9] and AIRDROP.[10]

Design Approach

A conceptual illustration of the subscale airfoil design procedure is shown in Fig. 1. First, a droplet impingement code was used to predict the droplet impingement limits. (The droplet impingement code, AIRDROP,[10] is discussed later.) Once the limits of impingement are known over the leading edge of the full-scale airfoil, that part of the full-scale airfoil geometry is fixed for the subsequent subscale airfoil shapes. For the sake of discussion, this fixed leading-edge section, which is common to both the full-scale airfoil and subscale airfoil, is referred to as the nose section, and the remaining section of the subscale airfoil profile is referred to as the aft section. The aft section of the subscale airfoil is then designed to provide full-scale flowfield and droplet impingement on the nose section of the subscale airfoil.

An initial geometry for the aft section is obtained through the use of a multipoint inverse airfoil design code[8] (PROFOIL). It is based on conformal mapping. The design of this intermediate airfoil, from which the aft section of the subscale airfoil is derived, is governed by several constraints, namely, the scale of the subscale airfoil, the upper and lower surface thickness and slope at the junction between the nose and aft sections (x_m, $\bar{x}_m$), and a desired form for the pressure recovery characteristics (x_r, $\bar{x}_r$). Apart from these constraints, additional continuity and closure constraints that form an integral part of the inverse design methodology[8] are also satisfied to achieve a physically possible design. A multidimensional Newton iteration scheme is further employed to satisfy additional constraints. The dependent and independent variables[8] used in the design are listed in Table 1. Once the constraints are satisfied, the aft section is combined with the nose section to form a subscale airfoil.

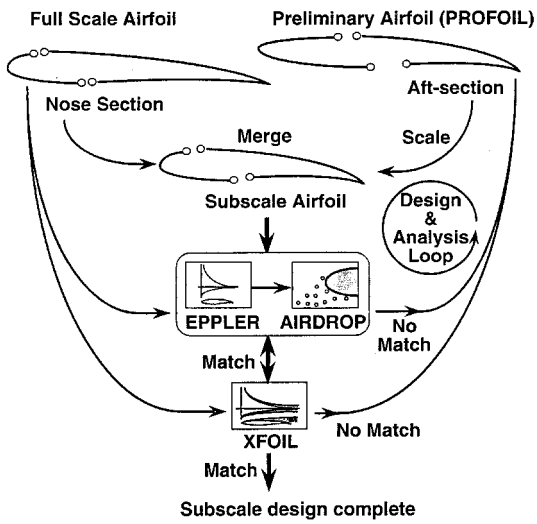

Fig. 1 Conceptual illustration of the subscale airfoil design procedure.

Table 1 Variables used in the design

Dependent variables	Independent variables
$K_S = 0.3$	ϕ_{le}
c_{m0}	v_1
$y(x_m)$	α^*
$y(\bar{x}_m)$	$\bar{\alpha}^*$

The potential flow over both the subscale and the full-scale airfoils is then analyzed using the Eppler code, which has the capability to analyze the potential flow over the airfoils using a method that employs panels with distributed surface singularities. The singularities used are vorticities distributed parabolically along each panel. Results predicted by the Eppler code have been shown to compare well with experiments.[14,15]

To have a physically similar flow and, therefore, similar droplet impingement in the vicinity of the nose section of both the subscale and the full-scale airfoils, the analysis is performed at the same angle of attack relative to the nose section chord of both airfoils. This is especially important in the case of large droplets. The local inviscid velocity distributions over the nose section and the stagnation point locations on both the subscale and full-scale airfoils are then compared. If the desired velocity distribution over the nose section and stagnation point location are not achieved, the aft section of the subscale airfoil is redesigned and again merged with the nose section to form a new subscale airfoil. The flow over the new subscale airfoil is then analyzed and compared with that over the full-scale airfoil. The process is repeated until the desired inviscid velocity distribution over the nose section and the stagnation point location is achieved.

In the next step, the subscale airfoil circulation, water droplet trajectories, and water droplet impingement characteristics are determined from AIRDROP,[10] an airfoil droplet impingement code that predicts droplet trajectories and the resultant impingement efficiency on single-element airfoils in incompressible flow. The code has been validated against NACA airfoil droplet impingement data and compares well when the cloud droplet size distribution is modeled correctly and the code is run matching the airfoil lift coefficient. Comparisons with predicted and measured rime ice accretion show good agreement.[10]

The numerical procedure employed by AIRDROP consists of two steps. First, the flowfield around the airfoil is determined by Woan's method,[16] which is based on Theodoreson's conformal mapping method. Second, single water droplet trajectories are calculated from the trajectory equation,[10] which in nondimensional form contains the three additional similarity parameters R_U, F_r, and K, apart from Re and M. Thus, given R_U, F_r, K, the droplet initial conditions, and the airfoil geometry, single water droplet trajectories are determined from the trajectory equation. Since an actual icing cloud has some distribution of droplet diameters, this distribution can be represented adequately by the volume median droplet diameter VMD; that is, the diameter about which one-half of the mass of water in the cloud is of droplet diameter greater than VMD and one-half less than VMD.

The individual droplet trajectories are combined to calculate the local impingement efficiency $\beta(=dy_0/dS)$. The impingement efficiency represents the dimensionless mass flux of impinging droplets at a point on the airfoil. Here, y_0 is the initial y displacement of an impinging droplet far ahead ($x_0 = -5c_{fs}$) of the airfoil. AIRDROP calculates a series of droplet trajec-

tories, fits a cubic spline through the y_0 vs S data points of the impinging droplets, and then computes the slope of the spline at a series of surface positions. This slope is β at that surface location. In this article, the y_0 vs S plot is referred to as the y_0 curve, and the β vs S plot is referred to as the β curve, and the term impingement characteristics refers to both the y_0 and β curves.

The impingement characteristics of both the full-scale and subscale airfoil are then compared. If the agreement in the impingement characteristics is poor, the subscale airfoil is modified and the design process is repeated again until good agreement is reached.

As will be shown, the amount of circulation plays a dominant role in determining the impingement characteristics through its impact on the flowfield, and therefore, the droplet trajectories. The expression for the total circulation can be derived from the relation

$$L = \rho V_\infty \Gamma = \tfrac{1}{2}\rho V_\infty^2 c C_l \tag{1}$$

which yields

$$\Gamma = \bar{\Gamma}/V_\infty c_{\text{fs}} = (c/2c_{\text{fs}})C_l \tag{2}$$

Therefore, the full-scale and subscale airfoil circulation is

$$\Gamma_{\text{fs}} = \tfrac{1}{2}C_{l,\text{fs}} \tag{3}$$

$$\Gamma_{\text{ss}} = (c_{\text{ss}}/2c_{\text{fs}})C_{l,\text{ss}} = (\eta/2)C_{l,\text{ss}} \tag{4}$$

respectively.

Finally, to obtain a well-designed subscale airfoil, consideration must also be given to viscous and compressibility effects to determine the true merits of the design. A discussion of the viscous considerations is presented in a later section.

Implementation

To expedite the design procedure, the Eppler code, PROFOIL, and AIRDROP were integrated into a single computer program. Then, the constraints on the subscale airfoil design were defined in terms of the fixed nose-section geometry, velocity distribution over the nose section, total circulation and the angle of attack relative to the nose section of the full-scale airfoil. To satisfy all of the previous constraints, numerous parametric trade studies were performed to help identify and isolate various key independent design variables. These independent variables were later identified as the coefficient c_{m0} of the airfoil from which the aft section of the subscale airfoil is derived, the scale η of the subscale airfoil, the angle γ, and the upper and lower surface pressure recovery locations.

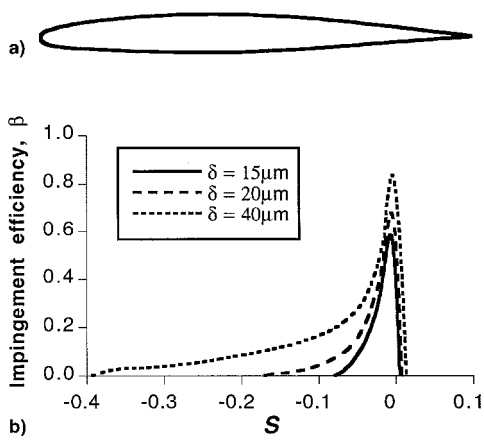

Fig. 2 a) Learjet 305 (GLC 305) airfoil and b) droplet impingement efficiency predicted by AIRDROP for the Learjet 305 airfoil.

To illustrate the effects of the independent design variables on the subscale airfoil design, the Learjet 305 (GLC 305) airfoil, shown in Fig. 2a, was selected as the full-scale airfoil along with the flight and icing conditions: V_∞ = 90 m/s (175 kn), $T = -5$°C, $Re = 6 \times 10^6$, M = 0.28, VMD = 15–40 μm, and α = 6 deg. At these conditions for the GLC 305 airfoil, AIRDROP predicts a lift coefficient $C_{l,\text{fs}} = 0.736$ and the circulation $\Gamma_{\text{fs}} = 0.368$. Figure 2b shows the corresponding β curves as predicted by AIRDROP. For VMD = 20 μm, AIRDROP predicts the limits of impingement as $S_u = 0.0076$ ($x/c = 0.0019$) on the upper surface and $S_l = -0.1822$ ($x/c = 0.1738$) on the lower surface.

Since the limits of impingement define the surface within which ice will accrete on the airfoil, only that part of the full-scale geometry needs to be fixed as the nose section for the subscale airfoil. The nose-section size is kept to a minimum, thereby, allowing more flexibility in the design of the aft section to satisfy the constraints. Thus, the nose-section geometry was selected as the full-scale airfoil surface from $x_m = x/c = 0.05$ on the upper surface to $\bar{x}_m = x/c = 0.20$ on the lower surface. Moreover, a half-scale ($\eta = 0.5$) subscale model was selected as the baseline case. Based on the size of the droplets under consideration, the effect of gravity on the droplets was considered to be negligible.

Most of the important effects can be examined by only considering inviscid effects; that is, boundary-layer displacement effects are second order relative to the effects of pitching moment, subscale airfoil chord length and the nose droop. Thus, the remainder of this section is divided into inviscid and viscous considerations.

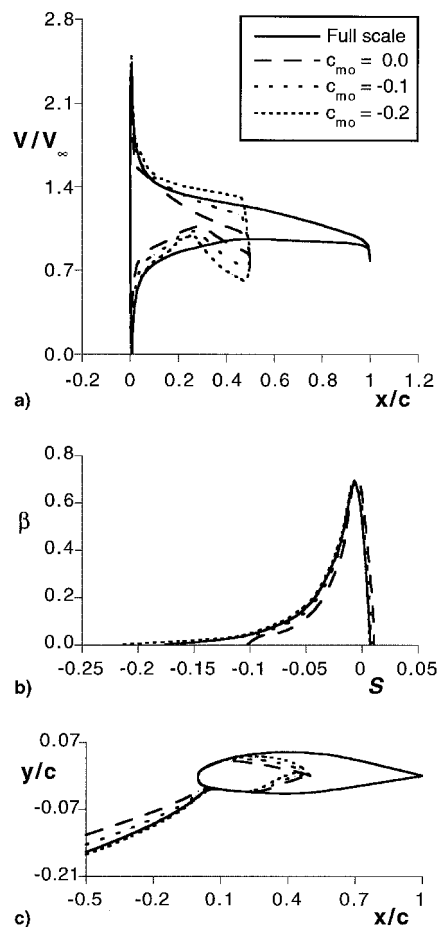

Fig. 3 Effect of pitching moment coefficient on a) the velocity distributions, b) droplet impingement efficiencies, and c) the tangent droplet trajectories.

Inviscid Considerations

Effect of Pitching Moment Coefficient

The effect of the pitching moment coefficient is illustrated in Fig. 3 in which an increase in the c_{m0} (more negative) results in a subscale airfoil with a greater aft camber and, therefore, a higher aft loading as well as an increase in the amount of circulation. The change in circulation with c_{m0} is found to be nearly linear, and a $c_{m0} = -0.2$ results in a subscale airfoil that has the same circulation as the full-scale airfoil. The droplet impingement characteristics also indicate a strong dependence on the value of circulation, which makes c_{m0} the main independent design variable. (Note that c_{m0} assumes the role of an independent design variable in the design of the aft section.) Figure 3c suggests that the subscale airfoil requires slightly less circulation than the full-scale airfoil to match the droplet trajectories. In particular, it was found that the subscale airfoil required 4.5% less circulation than the full scale to achieve full-scale droplet impingement characteristics. This can be attributed to the distribution of vorticity, which, in the case of a subscale airfoil, is more concentrated near the leading edge than in the case of the full-scale airfoil, resulting in a greater upwash in close proximity to the airfoil. Thus, a lower value of overall circulation is required to simulate full-scale droplet impingement.

Effect of Chord Length

To examine the effect of η on the design, subscale airfoils were designed for three different values of η, namely, 0.5, 0.7, and 0.9. Initially, the three subscale airfoils were designed such that they produced the same amount of circulation as the full-scale airfoil. The resulting velocity distributions, impingement characteristics, and the airfoil shapes are shown in Fig. 4. The results indicate that as the scale of the subscale model is reduced, the aft-loading on the airfoil increases significantly for it to produce the same amount of circulation. The mismatch in the impingement characteristics suggests that subscale models require less circulation to achieve full-scale impingement characteristics. Moreover, the results also suggest that the smaller the scale, the less circulation required to simulate full-scale droplet impingement characteristics. The subscale airfoils shown in Fig. 5 were designed such that the impingement characteristics were matched. The match in the impingement characteristics was achieved by designing subscale airfoils with reduced circulation as compared with the ones in Fig. 4. The results also indicate that the amount of circulation required to simulate full-scale droplet impingement vary from $0.955\Gamma_{fs}$ for $\eta = 0.5$ to $0.983\Gamma_{fs}$ for $\eta = 0.9$.

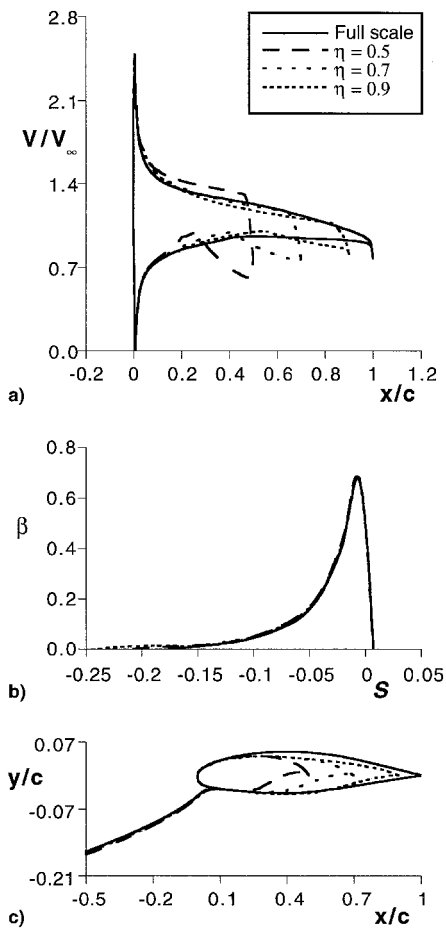

Fig. 4 Effect of chord length on a) the velocity distributions, b) droplet impingement efficiencies, and c) the tangent droplet trajectories at the matched circulation condition.

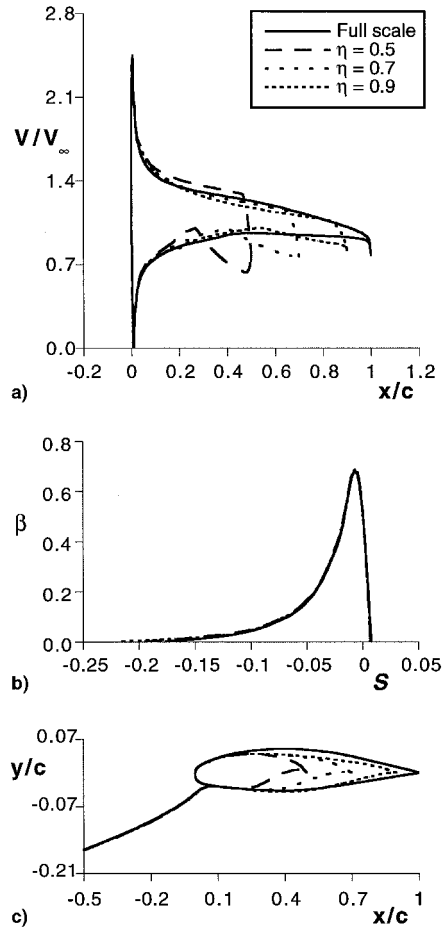

Fig. 5 Results showing a) the velocity distributions, b) droplet impingement efficiencies, and c) the tangent droplet trajectories at the matched impingement condition.

Effect of Nose Droop Angle

The effect of γ, shown in Fig. 6, becomes obvious from Fig. 7, which illustrates the usefulness of the nose droop in reducing the high aft-loading on airfoils. To keep the angle of attack relative to the nose section chord constant for both the full-scale and subscale airfoils, the subscale airfoil with a nose droop is analyzed at an effective angle of attack α_e, which takes into account the nose droop angle. As a result, the subscale airfoils with nose sections drooped downward are analyzed at higher angles of attack than those without the nose droop. Figure 7 shows the results of the subscale airfoil design with different nose droop angles for the same value of circulation as that of the half-scale model without the nose droop. The results indicate that the nose droop results in an increase

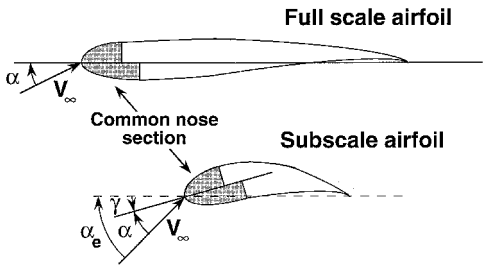

Fig. 6 Nose droop angle.

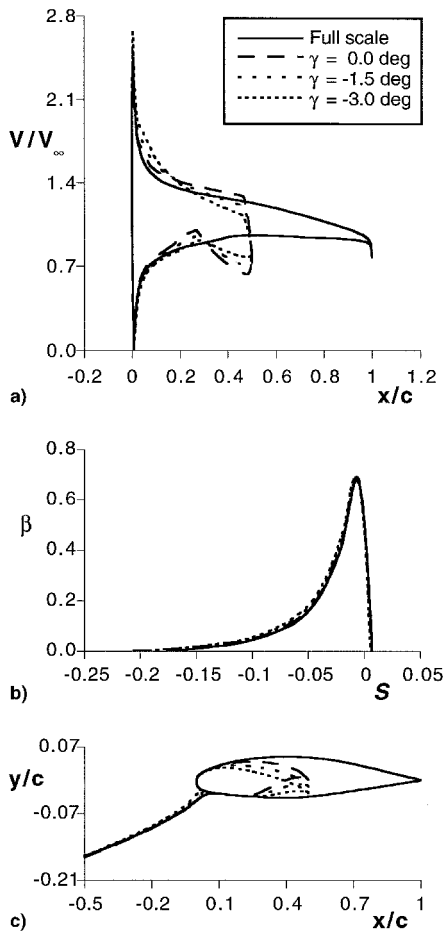

Fig. 7 Effect of nose droop on a) the velocity distributions, b) droplet impingement efficiencies, and c) the tangent droplet trajectories at the matched circulation condition.

in the camber of the subscale airfoil and, therefore, the subscale airfoil circulation. Moreover, the subscale airfoils with the nose drooped downward also operate at higher absolute angles of attack defined by α_e. As a result of this increase, the impingement characteristics show a mismatch. By decreasing the amount of circulation by an appropriate amount, the mismatch was removed as shown in Fig. 8. The reduction in the value of circulation as compared with that for the full-scale airfoil varies from $0.955\Gamma_{fs}$ for $\gamma = 0$ deg to $0.892\Gamma_{fs}$ for $\gamma = -3$ deg.

Other Effects

The upper and lower surface pressure recovery locations control to a great extent the shape of the airfoil near its trailing edge. Although, the effect of moving the pressure recovery locations results in a significant amount of improvement in the velocity distributions, and ultimately, the viscous characteristics, the change in the droplet impingement characteristics is, however, small.

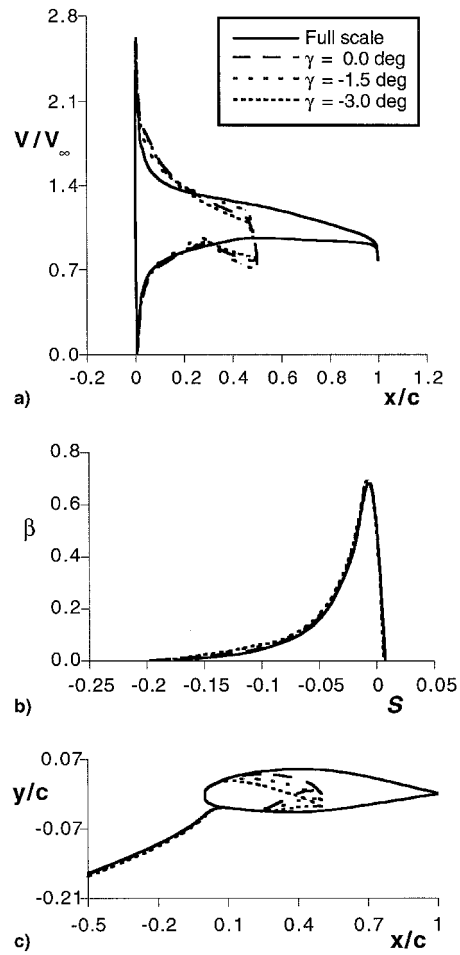

Fig. 8 Results showing a) the velocity distributions, b) droplet impingement efficiencies, and c) the tangent droplet trajectories at the matched impingement condition.

Summary of Inviscid Results

The previous study, based on inviscid considerations alone, illustrates the effect of different independent design variables on the subscale airfoil design. The results indicate that subscale airfoils require less circulation to simulate full-scale airfoil droplet impingement characteristics. The coefficient c_{m0} can be used effectively to achieve the desired amount of circulation. Since subscale airfoils tend toward high aft loading to simulate the desired impingement characteristics, a nose droop can be used effectively to offset the high aft loading to a large extent. The previous study also reveals that subscale airfoils with nose droop require even less circulation to achieve the desired impingement characteristics. Moreover, a subscale airfoil with a nose droop (downwards) must operate at a higher absolute angle of attack to simulate full-scale impingement characteristics over its nose section. Operation at high absolute angles of attack makes the subscale airfoil highly susceptible to flow separation, and therefore, it becomes necessary to evaluate the performance by means of a viscous analysis of the flowfield over the subscale airfoil.

Viscous Considerations

To determine the true merits of the design, a viscous flowfield analysis must form an essential part of the design. For the purpose of viscous flowfield analysis, XFOIL was used. XFOIL is a modified version of the ISES code,[17] which has been successfully applied to the design and analysis of airfoils for various applications that range from human-powered aircraft[18] to high and low Reynolds number transonic aircraft.[19,20] XFOIL uses a fully compatible laminar and turbulent viscous

formulation, a reliable transition formulation, and a global Newton iteration method to converge onto a flowfield solution.

The viscous analysis was performed to determine the effect of the presence of the viscous boundary on the flowfield. Typically inviscid flowfield codes overpredict the airfoil lift–curve slope and the lift on an airfoil as compared with viscous flow codes since, in a viscous flow, the presence of boundary layer decambers the airfoil and, therefore, reduces the C_l. This results in an error in the droplet trajectory calculation, since at the design angle of attack, the inviscid flowfield is for a higher lift coefficient and consequently greater circulation. To account for this effect, a procedure called the matched lift coefficient method is employed, in which the inviscid flowfield is analyzed at the lift coefficient that matches that of the viscous flowfield. A brief outline of this procedure as applied to the subscale airfoil design is as follows.

Initially, the viscous $C_{l,\text{fs}}$ is determined at the design angle of attack with the help of XFOIL. Using $C_{l,\text{fs}}$, an angle of attack $\alpha_{i,\text{fs}}$ is found such that running the inviscid flowfield code at $\alpha_{i,\text{fs}}$ produces an inviscid C_l that matches $C_{l,\text{fs}}$, the viscous C_l. Next, the inviscid flowfield as well as the droplet impingement characteristics of the full-scale airfoil are determined at $\alpha_{i,\text{fs}}$ and set as the target for the subscale airfoil design. A subscale airfoil is then designed to match the target flowfield and impingement characteristics. Once a match is achieved, a viscous analysis of the subscale airfoil is performed at the matched conditions to determine the viscous $C_{l,\text{ss}}$. As in the full-scale airfoil case, an inviscid $\alpha_{i,\text{ss}}$ is calculated and used to determine the inviscid flowfield and droplet impingement characteristics for comparison with the target flowfield and droplet impingement characteristics. If the desired characteristics are achieved, the design is complete, otherwise, the subscale airfoil is modified and the whole process is repeated again until the desired match is achieved.

Design Example

In this section, a specific design example is presented with the objective to design a half-scale model of the GLC 305 airfoil to simulate full-scale droplet impingement. Table 2 lists the flight and icing conditions for the final design, whereas Table 3 lists the final values of the design variables for the converged solution. The subscale airfoil was designed with τ = 6 deg. The effects as a result of compressibility were also considered during the viscous flow analysis of both airfoils.

Figure 9 shows the comparison between the inviscid velocity distributions for the converged solution at α_e = 6 deg together with the comparison between the velocity distributions (viscous) at the design conditions, where, $C_{l,\text{fs}}$ = 0.7690 and $C_{l,\text{ss}}$ = 1.2148. The respective inviscid velocity distributions for the matched lift coefficient case are shown in Fig. 10a. All of the figures show good agreement in velocity distribution over the common nose section. The comparison of the impingement characteristics corresponding to the respective matched lift coefficient cases is shown in Fig. 10b, whereas, a comparison of tangent droplet trajectories is shown in Fig. 10c. The results indicate excellent agreement in impingement efficiency. The

Table 2 Design flight and icing conditions

Variable	Full scale	Subscale
V_∞, m/s	87	87
T, °C	−5	−5
Re	6×10^6	3×10^6
M	0.28	0.28
c, m	1.0	0.5
VMD, μm	20	20
α, deg	6	6
γ, deg	0	−3
α_e, deg	6	9

Table 3 Converged solution

Dependent variables	Independent variables
K_S = 0.3	ϕ_{1e} = 189.53 deg
c_{m0} = −0.065	v_1 = 2.133
$y(x_m = 0.05)$	α* = 8.93, 11.93, and 14.93 deg
$y(\bar{x}_m = 0.20)$	$\bar{\alpha}$* = 1.17 deg (all segments)
τ = 6 deg	$x_r = 0.0114c$, $\bar{x}_r = 0.4746c$

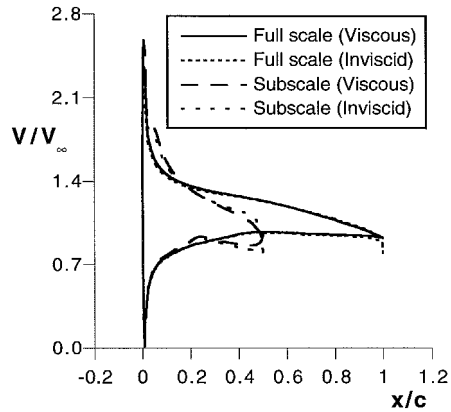

Fig. 9 Comparison between the inviscid velocity distribution at α_e = 6 deg together with the comparison between the velocity distribution at the design conditions listed in Table 3.

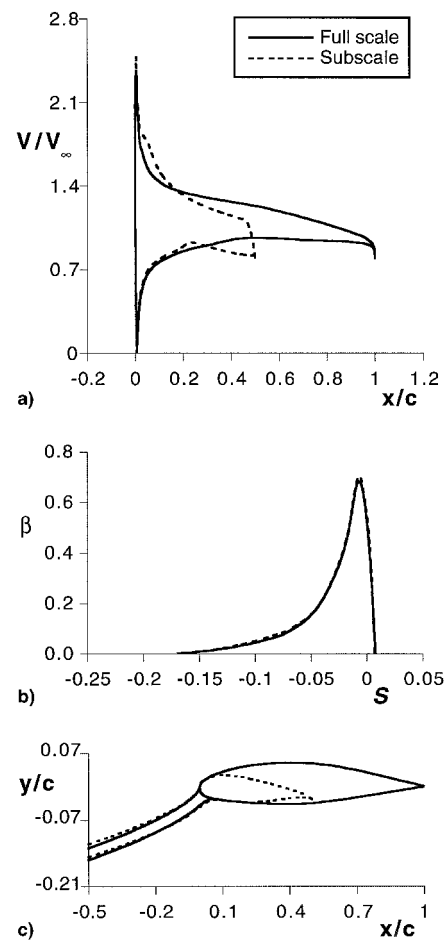

Fig. 10 Comparison between a) the velocity distributions, b) droplet impingement efficiencies, and c) the tangent droplet trajectories at $\alpha_{i,\text{fs}}$ and $\alpha_{i,\text{ss}}$, corresponding to the respective matched lift coefficients.

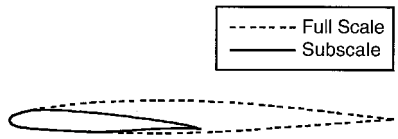

Fig. 11 Final subscale airfoil and the Learjet 305 airfoil.

tangent droplet trajectories, although originating at different locations along the y axis, are matched in the vicinity of the leading edge. This is consistent with the observations made during the case studies that subscale airfoils require a lower value of circulation to achieve full-scale droplet impingement characteristics. The final subscale airfoil and the Learjet 305 airfoil are shown in Fig. 11.

Conclusions

Several important conclusions can be drawn from this study. First, it is shown that subscale airfoils with full-scale leading edges can be designed to exhibit full-scale droplet impingement and, therefore, ice accretion. Second, the results indicate that subscale airfoils require less circulation to simulate full-scale airfoil droplet impingement characteristics. The pitching moment coefficient of the airfoil from which the aft section for the subscale airfoil is derived can be used effectively to achieve the desired amount of circulation on the subscale airfoil. Third, since subscale airfoils tend toward high aft loading to simulate the desired droplet impingement characteristics, a nose droop can be used effectively to offset the high aft loading. Fourth, an airfoil with a nose droop (downwards) must operate at a higher absolute angle of attack to keep the same angle of attack relative to its nose section as the full-scale airfoil to simulate full-scale impingement characteristics. Operation at high absolute angles of attack makes the subscale airfoil highly susceptible to flow separation, and therefore it becomes necessary to integrate the viscous analysis of the flowfield over the subscale airfoil into the design process. Fifth, to incorporate viscous and compressibility effects, the matched lift coefficient method outlined in this article was applied successfully in the final design example.

Acknowledgments

This work has been sponsored by NASA Lewis Research Center under Grant NCC3-408. Helpful discussions with Tom Ratvasky, Gene Addy, and Tom Bond of NASA Lewis Research Center are gratefully acknowledged. We would also like to thank Reuben Chandrasekharan of Learjet Inc. for providing NASA Lewis Research Center with the Learjet GLC 305 airfoil used in this study.

References

[1]Hauger, H. H., and Englar, K. G., "Analysis of Model Testing in an Icing Wind Tunnel," Douglas Aircraft Co., SM 14993, May 1954.

[2]Sibley, P. J., and Smith, R. E., Jr., "Model Testing in an Icing Wind Tunnel," Lockheed Aircraft Corp., LR 10981, Oct. 1955.

[3]Langmuir, I., and Blodgett, K., "A Mathematical Investigation of Water Droplet Trajectories," U.S. Army Air Forces, TR 5418, Feb. 1946.

[4]Von Glahn, U. H., "Use of Truncated Flapped Airfoils for Impingement and Icing Tests of Full-Scale Leading-Edge Sections," NACA RM E56E11, July 1956.

[5]Perkins, P., and Rieke, W., "Aircraft Icing Problems—After 50 Years," AIAA Paper 93-0392, Jan. 1993.

[6]Eppler, R., "Direct Calculation of Airfoils from Pressure Distribution," NASA TT F-15, 417, March 1974; Translated from *Ingenieur-Archive* , Vol. 25, No. 1, 1957, pp. 32–57.

[7]Eppler, R., *Airfoil Design and Data*, Springer–Verlag, New York, 1990.

[8]Selig, M. S., and Maughmer, M. D., "A Multipoint Inverse Airfoil Design Method Based on Conformal Mapping," *AIAA Journal*, Vol. 30, No. 5, 1992, pp. 1162–1170.

[9]Drela, M., "XFOIL: An Analysis and Design System for Low Reynolds Number Airfoils," *Lecture Notes in Engineering: Low Reynolds Number Aerodynamics*, edited by T. J. Mueller, Vol. 54, Springer–Verlag, New York, June 1989, pp. 1–12.

[10]Bragg, M. B., "Rime Ice Accretion and Its Effect on Airfoil Performance," Ph.D. Dissertation, Ohio State Univ., Columbus, OH, 1981.

[11]Bragg, M. B., "The Effect of Geometry on Airfoil Icing Characteristics," *Journal of Aircraft*, Vol. 21, No. 7, 1984, pp. 505–511.

[12]Bragg, M. B., "A Similarity Analysis of the Droplet Trajectory Equation," *AIAA Journal*, Vol. 20, No. 12, 1982, pp. 1681–1686.

[13]Ruff, A. G., and Berkowitz, B. W., "User's Manual for the NASA Lewis Ice Accretion Prediction Code (LEWICE)," NASA CR 185129, May 1990.

[14]Somers, D. M., "Design and Experimental Results for a Flapped Natural-Laminar-Flow Airfoil for General Aviation Application," NASA TP-1865, June 1981.

[15]Maughmer, M. D., and Somers, D. M., "Design and Experimental Results for a High-Altitude, Long Endurance Airfoil," *Journal of Aircraft*, Vol. 26, No. 2, 1989, pp. 148–153.

[16]Woan, C. J., "Fortran Programs for Calculating the Incompressible Potential Flow About a Single Element Airfoil Using Conformal Mapping," Ohio State Univ., TR AARL 80-02, Columbus, OH, Jan. 1980.

[17]Drela, M., and Giles, M. B., "ISES: A Two-Dimensional Viscous Aerodynamic Design and Analysis Code," AIAA Paper 87-0424, Jan. 1987.

[18]Drela, M., "Low-Reynolds Number Airfoil Design for the MIT Daedalus Prototype: A Case Study," *Journal of Aircraft*, Vol. 25, No. 8, 1988, pp. 724–732.

[19]Giles, M. B., and Drela, M., "A Two-Dimensional Transonic Aerodynamic Design Method," *AIAA Journal*, Vol. 25, No. 9, 1987, pp. 1199–1206.

[20]Drela, M., and Giles, M. B., "Viscous-Inviscid Analysis of Transonic and Low Reynolds Number Airfoils," *AIAA Journal*, Vol. 25, No. 10, 1987, pp. 1347–1355.